Variation process in stiffness inferred by nonlinear inversion during mainshocks at Kushiro Port vertical array site

Mostafa Thabet[1], Hiroo Nemoto[2], and Koichi Nakagawa[1]

[1]*Department of Geosciences, Graduate School of Science, Osaka City University, Osaka, Japan*
[2]*School of Math and Natural Science, J. F. Oberlin University, Tokyo, Japan*

In the present study, a set of three strong motions accompanied by 21 before and after mainshock motions from liquefed soil at the Kushiro Port vertical array site have been obtained. *S*-wave velocity variation is estimated using a new proposed nonlinear GA inversion technique. This inversion technique is reproductive in assessment for *S*-wave velocities due to its direct link with the simulation FEM program and matching technique between the observed and simulated waveforms. Layers (6 ∼ 23 m depth) have been found to be responsible for liquefaction at the Kushiro Port site. Stiffness degradation due to liquefaction could be predicted by applying the inversion technique on the horizontal components of the mainshocks at different time-windows and then multiplying the weighting functions by the nonlinear simulated ground motions. These weighting functions were applied to delete the misfit time window of the nonlinear simulated ground motions when these were compared to the observed records. Finally, stacking was applied for the weighted nonlinear simulated ground motions. A strong degree of liquefaction is concluded during the Kushiro-Oki (1993) and the Hokkaido Toho-Oki (1994) earthquakes, whereas a low degree of liquefaction was detected to have occurred during the Tokachi-Oki (2003) earthquake due to high increase of rigidity following a trend that resembles a consolidation curve.
Key words: Strong motions, Kushiro Port vertical array site, stiffness degradation, nonlinear inversion.

1. Introduction

Analysis of the observed ground motion during or immediately after an earthquake forms the backbone of the development of earthquake monitoring and early damage assessment systems. Ground motion parameters from liquefied-soil sites have been examined in a number of studies which have employed several methods for assessing liquefaction based on strong motion records. Nakayama *et al.* (1998), Miyajima *et al.* (1998), Ozaki (1999), and Kostadinov and Yamazaki (2001) reported various methods that consider ground motion parameters such as peak horizontal ground acceleration, maximum spectrum intensity, and maximum horizontal ground displacement. The respective method evaluates the occurrence of liquefaction either positively or negatively if these parameters exceed certain limit values.

Since the nonlinear effect typically occurs in unconsolidated soft soils, our analysis should be focused on very surficial layers. In this study, modification of subsurface stiffness structure associated with successive mainshocks at Kushiro Port were examined using a newly developed genetic algorithm inversion technique. This technique is able to assess the occurrence of liquefaction through an evaluation of stiffness degradation during strong shaking. It is therefore possible to identify the nonlinear behavior and changes in the physical properties in the layers with the lapsed time. The results are discussed in detail and compared with the observed records.

2. Data

Kushiro City is a medium-sized city located on the eastern part of Hokkaido, Japan. As shown in Fig. 1, the lithology at Kushiro Port downhole array site can be divided to four main units. (1) coarse sand layers intercalated with thin sandy gravel layers (0 m ∼ 22 m depth), (2) fine sand layers intercalated with silt layers (22 m ∼ 46 m depth), (3) sandy gravel layers intercalated with coarse sand layers (46 m ∼ 52 m depth), and (4) fine sand layers intercalated with coarse sand layers (52 m ∼ 77.45 m depth).

Records of the three mainshocks—the 1993 Kushiro-Oki, the 1994 Hokkaido Toho-Oki, and the 2003 Tokachi-Oki earthquakes—accompanied with 21 before and after mainshocks observed at depths of 0 m and 77.45 m were obtained from the Port and Airport Research Institute, as shown in Table 1. The data were recorded using the digital ERS-GV strong-motion seismograph as acceleration with Gal units, with a sampling frequency of 100 Hz. The epicenter locations for these events are shown in Fig. 2 with their hypocenter distribution. In the present study, we focus on the role of the *S*-waves in the horizontal components of all events. By applying Snell's law, we were able to calculate incident angles for all the events using the Koketsu *et al.* (2003) velocity structure. Therefore, vertical propagation for the seismic waves is assumed because the incidence angles for all the events lie between 88.2° ∼ 89.8°.
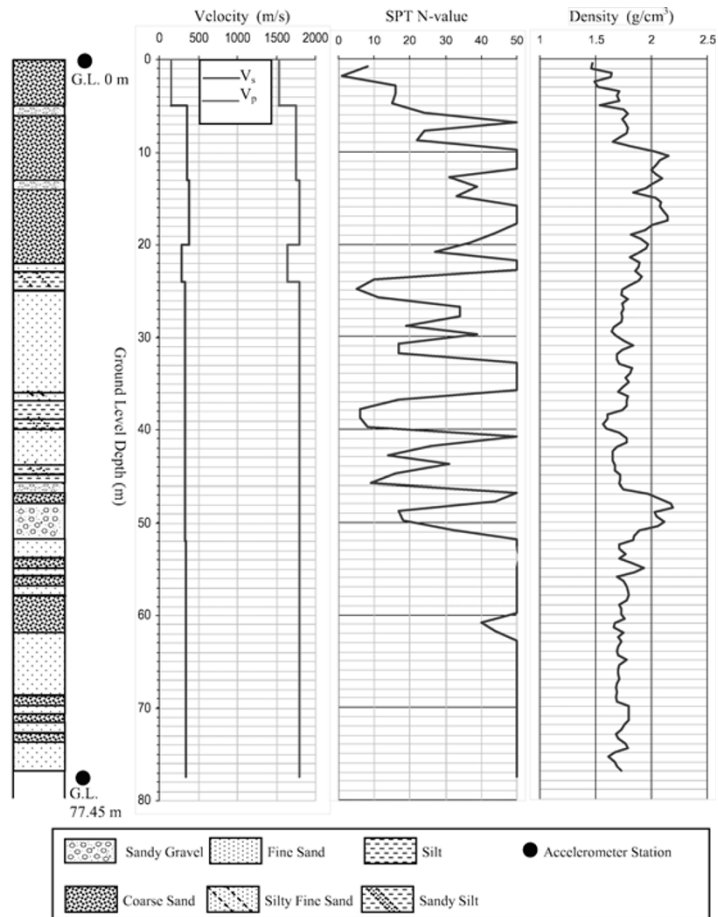
Fig. 1. Soil properties at Kushiro Port vertical array site. V_p and V_s are the primary and shear wave velocities, respectively.
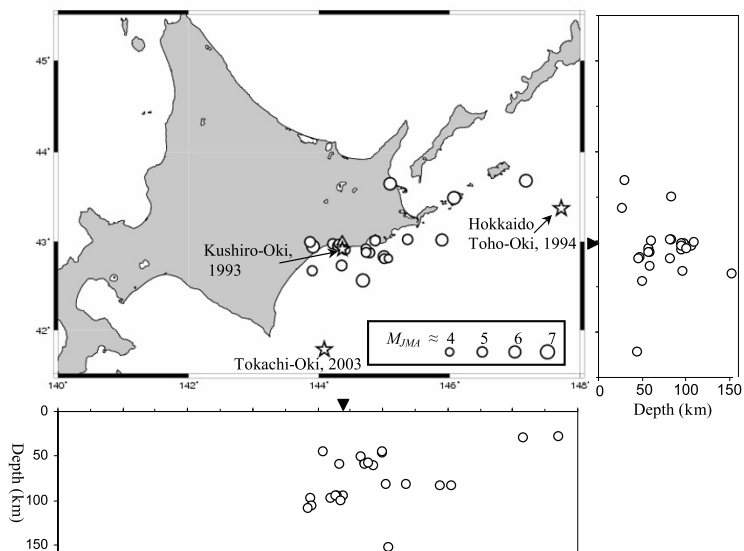

Fig. 2. Epicenter location for events shown in Table 1 with their hypocenter distribution. The triangle, star and circle denote the Kushiro Port vertical array site, mainshock and before or after mainshock event, respectively.

3.   Nonlinear Inversion Technique

Genetic algorithms (GA) have proven themselves as reliable computational search and optimization procedures for complex objectives invloving large number of variables. In the present study, the objective function for the GA inversion comprises of two main successive steps. Firstly, simulations are conducted by AMPLE2000 (a one-dimensional finite element method based dynamic analysis code, after

Table 1. Groundmotions recorded at Kushiro Port array site.

Origin time	Latitude	Longitude	Depth (km)	Magnitude	Epicentral distance (km)
5/19/2005　1:33	42°55.2′	144°43.2′	58.2	4.8	30.5
3/12/2005　3:47	43°00.7′	144°51.6′	61	5.1	40.7
4/12/2004　3:06	42°49.9′	144°59.7′	47	5.8	54.7
10/ 8/2003 18:06	42°33.8′	144°40.4′	51	6.4	54.5
9/27/2003 17:06	42°44.0′	144°20.8′	59	5.2	29.2
9/26/2003　8:11	42°48.6′	145°00.0′	46	4.8	56
9/26/2003　4:50	41°46.6′	144°04.9′	45	8	137.4
9/11/2003　4:31	42°40.4′	143°53.7′	97	4.9	52.1
4/27/2001　2:48	43°01.2′	145°52.9′	83.1	5.9	123.7
6/13/2000　1:54	42°52.8′	144°43.3′	58.8	4.7	32.1
5/13/1999　2:59	42°56.7′	143°54.5′	106	6.3	39.5
11/15/1997 16:05	43°38.8′	145°05.3′	153.1	6.1	93.3
6/15/1997 13:54	42°58.6′	144°12.7′	97.6	5.1	12.2
5/ 6/1996 17:21	42°54.4′	144°24.2′	94.8	4.5	10.5
9/16/1995　8:52	42°59.9′	143°51.7′	109.7	5.2	40.4
10/ 6/1994　5:39	43°40.9′	147°10.2′	30	6.3	239.5
10/ 4/1994 22:22	43°22.3′	147°42.7′	28	8.2	274.6
8/31/1994 18:07	43°29.4′	146°04.1′	83.6	6.3	148.8
6/ 3/1993 17:01	42°48.7′	145°03.7′	81.6	4.1	60.7
3/31/1993　6:43	43°01.6′	145°21.4′	82.8	5.1	81.1
3/12/1993　1:27	42°58.7′	144°17.8′	95.2	4.3	5.5
2/ 4/1993 23:43	42°57.2′	144°16.9′	94.7	4.8	7.9
1/15/1993 20:06	42°55.0′	144°21.4′	100.6	7.5	8.8
11/30/1992　9:20	42°52.6′	144°46.6′	57.6	4.9	36.4

Pestana and Nadim, 2000). These simulations were conducted using velocity models selected by GA. Observed motions at a depth of 77.45 m are used as input motions in the simulation program. In linear analysis the soil is assumed to be a linear inelastic material with properties controlled by small strain shear stiffness, whereas in nonlinear analysis, simulations are performed using a hyperbolic failure-seeking model that was introduced by Pyke (1979).

After each simulation, matching is performed between the simulated motion and their corresponding observed motion at the surface. For this purpose, a new proposed quantitative matching technique is presented. This matching technique consists of a successive series of equations to find a quantitative measure for the non-fitting between the simulated and observed motions (i.e. Error); see Eqs. (1) through (4).

$$\sigma_i = \sqrt{\left(A_{i(\text{simulated})} - A_{i(\text{observed})}\right)^2} \qquad (1)$$

$$\text{Aveg.} = \frac{\sum\limits_{i=1}^{\text{ndata}} \sigma_i}{\text{ndata}} \qquad (2)$$

$$\sigma_{\text{Total}} = \sqrt{\frac{\sum\limits_{i=1}^{\text{ndata}} (\sigma_i - \text{Aveg.})^2}{\text{ndata}}} \qquad (3)$$

$$\text{Error} = \text{Aveg.} + \sigma_{\text{Total}} \qquad (4)$$

where $A_{i(\text{simulated})}$ and $A_{i(\text{observed})}$ are the amplitude of the simulated and observed motions, respectively, ndata is the number of the data points in the selected time window for matching, i is the time series data points starting from 1 through ndata, Error is the error in matching between observed and simulated motions.
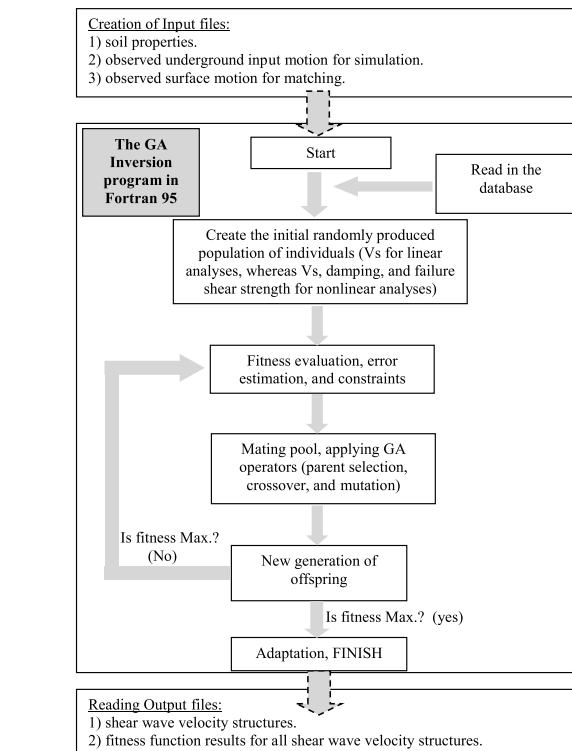
Consequently, the lesser the error in matching for a given shear wave velocity structure, the higher the fitness between the individuals. We adopted and modified the backbone

Fig. 3. Flowchart for the nonlinear GA inversion technique. The database consists of the minimum and maximum of V_s structure and GA parameters, such as mutation and crossover probability and the string length.
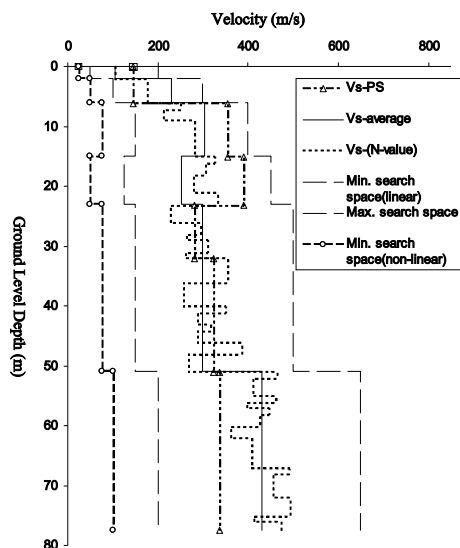
Fig. 4. Averaged initial shear wave velocity structure and the search space for GA inversion used in linear and nonlinear analyses at the Kushiro Port array site. V_s-PS and V_s-(N-value) are the shear wave velocity estimated from PS logging data and estimated empirically from the N-value, respectively.
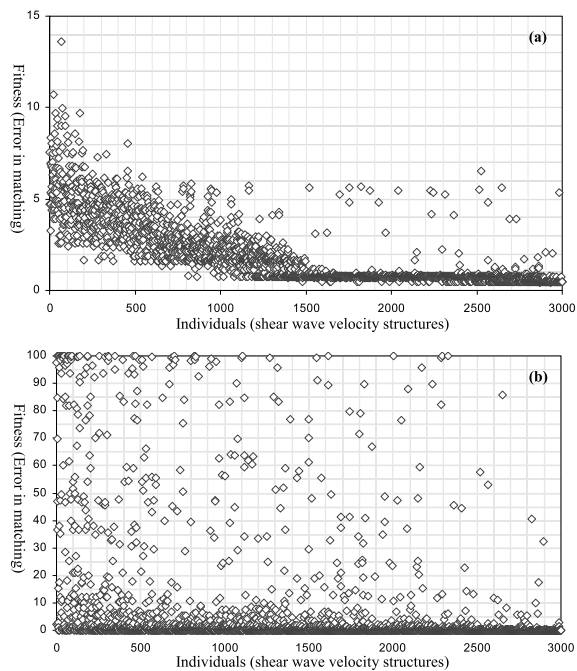

Fig. 5. Example of GA inversion performance during linear analyses using the currently proposed matching technique (a), and using the chi-square matching method (b).
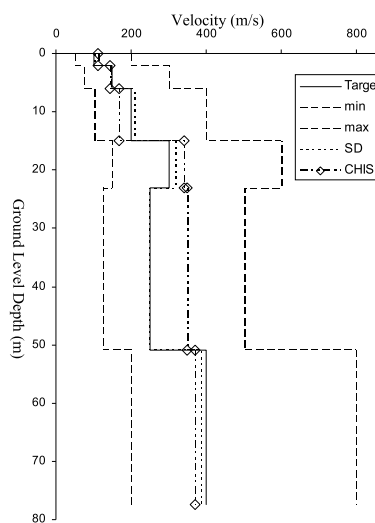

Fig. 6. Resulting shear wave velocity structures from the experimental analyses using the currently proposed matching technique (SD) and using the chi-square matching method (CHIS). Target, min and max are the target shear wave velocity, and minimum and maximum search space respectively, in the experimental analyses.

genetic algorithm routines from the LGADOS code placed in a public domain by Coley (2001, 2002). A flowchart for the nonlinear GA Inversion technique is shown, in Fig. 3.

After several trials, we concluded that the population of 100 individuals and 30 generations produce an appropriate performance of the algorithm. One individual corresponds to one simulation using one shear velocity model. In the case of linear simulations, the genes for each individual are shear wave velocities for each layer. In the case of nonlinear simulations, the genes for each individual are shear wave velocities, damping coefficients, and failure shear strength for each layer. The maximum standard deviation for the layers (0 ∼ 23 m depth) is 64 m/s, whereas for the layers below the depth of 23 m it is 11 m/s. Therefore, the layers below the depth of 23 m are not highly responsible for the nonlinear response. It is important to note that during nonlinear simulations the velocities for these layers are fixed.

The designed search space for the linear analyses is ±50% of the initial shear wave velocities, whereas the designed minimum search space for the nonlinear analyses is 75% reduced from the initial shear wave velocities for each layer, as shown in Fig. 4. The maximum search space for the nonlinear analyses is similar for that for the linear analyses because during nonlinear analyses a reduction in shear velocities is expected. This initial shear wave velocity structure was estimated based on velocities obtained empirically from the (SPT)N-value (after Thabet *et al.*, 2007). In GA searching, the incremental value of the model parameter is variant because the values are selected stochastically and governed by the fitness function. According to typical modulus reduction and damping curves for sand at a depth of less than 100 m (after Seed *et al.*, 1984), the damping factor applied in the linear analysis is equal to 1%, whereas damping factors during nonlinear analysis are permitted in the range between approximately 3 and 30%. For the inversion of the velocities before and after the three mainshocks,

the EW and NS components are treated independently.

4. Validation of the Analyses

An experimental validation has been conducted to verify the reproductivity of the newly proposed nonlinear GA inversion technique. For this purpose, we used the underground NS component of the before 1993 Kushiro-Oki earthquake as an input motion to calculate the motion at the surface using assumed velocity structure. Experimentally, we consider the calculated motion at the surface and the assumed velocity structure as experimental targets. GA
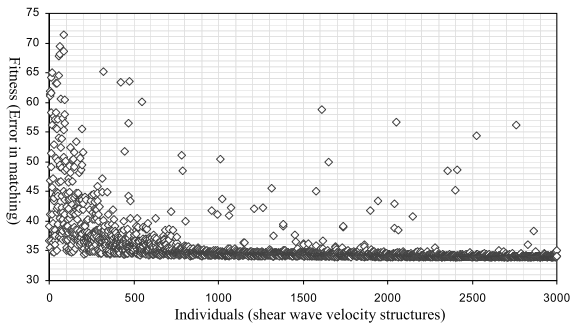
Fig. 7. Example of GA inversion performance using the current proposed matching technique during the nonlinear analyses.

Fig. 8. Frequency-Time representation for the NS component of the 1993 Kushiro-Oki earthquake.

inversion is then carried out to find the velocity structure that can yield 100% matching between the experimentally calculated surface motion and the simulated motions resulted from GA inversion. An example of GA inversion performance for the before mainshock event using the currently proposed matching technique and chi-square matching method is shown in Fig. 5. The highest difference between the experimental velocity structure and the resulting velocity structure from GA inversion using the current proposed matching technique is 5%, whereas using the chi-square matching method, it is 40%, as shown in Fig. 6.

Similar experimental analyses are conducted using nonlinear simulations. An example of the GA performance is shown in Fig. 7. The standard error using nonlinear simulations is approximately 20%. This high standard error compared with those related to linear simulations can be attributed to the three unknown factors (shear velocities, damping ratio, and failure shear strength) that we are searching for in the nonlinear simulations. The results from the currently proposed nonlinear GA inversion technique are considered to be unique results for five main reasons. (1) the above-mentioned experimental analyses, (2) a direct link between the GA inversion with the FEM simulation and matching technique due to the high dependency of ground motion simulation on a reliable shear wave velocity structure, (3) limiting the shear wave velocity search space to ±50% of the initial velocity model, (4) very small dispersion that resulted from the experimental validation for the inversion technique is about ±5% error, (5) high consistency of the resulted shear velocities inferred from 21 before and after mainshock events for layers below at a depth 23 m that do not contribute to the nonlinear response.

5.   Liquefaction Detection Technique

After the shear wave velocity structures were estimated from before and after the mainshocks, nonlinear analyses for the three mainshocks were carried out. For this purpose, each mainshock is divided into four time windows, each of which along the mainshock time series is treated as an independent ground motion. The first time window is determined based on the frequency-time representation of the mainshock motion at the surface, as shown in Fig. 8, whereas the later three time windows are determined based on the dominant peak ground accelerations with a lapse of time du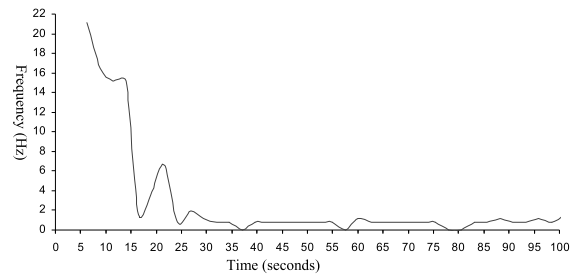ring each specific time window. The frequency-time representation is calculated by taking the Fourier transform within a moving time window, known also as the short-time Fourier transform (STFT), which is the simplest among the variety of time-frequency representations (Qian and Chen, 1996). In the present study, the STFT computation is conducted for the mainshock horizontal acceleration records utilizing a Hanning window of length 2.56 s. Based on the fact that the soil shows degradation behavior at strains larger than 1%, a number of nonlinear simulations are carried out for each independent time window along the mainshock time series using the nonlinear GA inversion technique to set the parameters required for nonlinear analyses, such as failure shear strength and damping ratio and shear velocities for each layer. The parameters in Table 2 represent the best fit parameters in our simulations for the 1993 Kushiro-Oki earthquake. It is important to note that shear wave velocities and failure strength values of the fifth and sixth layers are fixed. We fixed these layers based on results from earlier linear analyses that showed that these layers are not highly responsible for the nonlinear response that appeared at the surface horizontal components. In order to minimize both the search space and time, the damping ratios of the layers below the depth of 23 m were set between 1 and 5% according to typical modulus reduction and damping curves for sand at a depth of less than 100 m (after Seed *et al.*, 1984). The horizontal components observed at the 77.45 m depth were used as imposed motions in the simulations. The simulated motions were subsequently multiplied by weighted functions in order to eliminate the non-fitting part of the simulated motion. These weighted functions had a summation of one at any time step. Finally, stacking of the simulated weighted waveforms is applied.

6.   Results and Discussion

Good agreement is obtained in terms of the frequency content, amplitude, and waveform between the observed and simulated motions for the 21 before and after mainshock events. An example of simulated waveforms for an after the 1994 Hokkaido Toho-Oki mainshock event that achieved the best fit with the observed motions in each of the EW and NS components is shown in Fig. 9.

The final velocity structures are shown in Fig. 10. These velocity structures represent the averaged structures for the periods before, between, and after the three mainshocks. Shear wave velocity structures from the EW and NS components can be identical only in the case of an isotropic medium, but in practical terms they are different due to het-

Table 2. Resulted nonlinear parameters used for the 1993 Kushiro Oki earthquake. ζ and γ are damping ratio and shear strength, respectively.

| Time window	Depth	EW component			NS component		
		V_s (m/s)	ζ (%)	γ (kPa)	V_s (m/s)	ζ (%)	γ (kPa)
First time window	0 m ~ 2 m	123	3.3	1.65 E05	123	6	2.21 E05
	2 m ~ 6 m	288	3.3	9.60 E05	213	6	7.04 E05
	6 m ~ 15 m	155	5	3.00 E05	159	11	3.55 E05
	15 m ~ 23 m	280	5	1.00 E06	280	11	1.13 E06
	23 m ~ 51 m	280	3	1.40 E06	280	4	1.40 E06
	51 m ~ 77.45 m	333	3	1.93 E06	333	4	1.93 E06
Second time window	0 m ~ 2 m	169	14	2.79 E05	156	12	2.73 E05
	2 m ~ 6 m	218	14	4.94 E05	181	12	3.91 E05
	6 m ~ 15 m	125	15	1.64 E05	174	15	3.12 E05
	15 m ~ 23 m	143	15	2.20 E05	106	15	1.19 E05
	23 m ~ 51 m	280	2.3	1.40 E06	280	3	1.40 E06
	51 m ~ 77.45 m	333	2.3	1.93 E06	333	3	1.93 E06
Third time window	0 m ~ 2 m	185	15	3.62 E05	190	4	3.27 E05
	2 m ~ 6 m	210	15	4.97 E05	278	4	7.46 E05
	6 m ~ 15 m	108	15	1.12 E05	82	11	1.28 E05
	15 m ~ 23 m	100	15	9.87 E04	140	11	3.83 E05
	23 m ~ 51 m	280	2.4	1.40 E06	280	3	1.40 E06
	51 m ~ 77.45 m	333	2.4	1.93 E06	333	3	1.93 E06
Fourth time window	0 m ~ 2 m	158	5	2.85 E05	191	3	4.89 E05
	2 m ~ 6 m	254	5	7.84 E05	277	3	1.09 E06
	6 m ~ 15 m	63	23	7.60 E04	66	25	8.29 E04
	15 m ~ 23 m	124	23	3.02 E05	230	25	1.03 E06
	23 m ~ 51 m	280	4	1.40 E06	280	5	1.40 E06
	51 m ~ 77.45 m	333	4	1.93 E06	333	5	1.93 E06
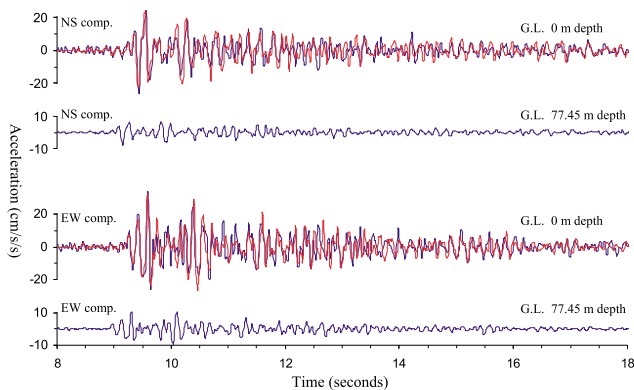
Fig. 9. Linear simulations of the 2003/9/11 04:31 acceleration records, observed (blue traces) and simulated (red traces).

erogeneity in the medium according to analyses conducted by Aguirre and Irikura (1997). Therefore, the two components are treated independently. Layers (0 ~ 6 m depth) show unstable variation in shear velocities before and after the 1993 Kushiro-Oki earthquake that could be assumed to be due to the consolidation recovery process that follows the nonlinear response of the mainshock. The layers (6–23 m depth) exhibit a strong suppression of shear wave velocity in both components of the aftershocks. The maximum reductions in shear velocities before and after the 1993 Kushiro-Oki and 1994 Hokkaido Toho-Oki earthquakes are 20 and 24%, respectively, whereas the maximum reduction in shear velocities before and after the 2003

Tokachi-Oki is 6%. The standard deviations of the differences between the velocities of before and after the three mainshocks are calculated at intervals of 0 ~ 23 m depth and 23 ~ 77.45 m depth. At 0 ~ 23 m depth, the maximum standard deviation is 64 m/s. At 23 ~ 77.45 m depth, the maximum standard deviation is 9 m/s. Shear velocities at a depth of 23 ~ 51 m estimated from the NS component of the 1993 Kushiro-Oki earthquake and those of a depth of 51 ~ 77.45 m depth that estimated from the NS component of the 1994 Hokkaido Toho-Oki earthquake and EW component of the 2003 Tokachi-Oki earthquake show an unusual maximum standard deviation of 18 m/s. This can be assumed to be due to the incompletely uniqueness of the analysis.

In the nonlinear analyses, the resultant waveforms are in strong agreement with the observation in the designed time windows. An example of the nonlinear simulations for the 1993 Kushiro-Oki earthquake with their corresponding time windows is shown in Fig. 11. From the STFT computation and from the nonlinear analysis that was carried out, we could assume that the first time window shows the starting point for the liquefaction, whereas the second and third time windows are the most influenced by the liquefaction. The misfit that appears outside the designed time windows is natural because the present nonlinear constitutive model that was introduced by Pyke (1979) does not account for liquefaction effects. This nonlinear constitutive model is shown in Eq. (5).

$$\tau - \tau_{\mathrm{c}} = G_{\max} \cdot \frac{(\gamma - \gamma_{\mathrm{c}})}{(1 + (\gamma - \gamma_{\mathrm{c}})/(C \cdot \gamma_{\mathrm{ref}}))} \qquad (5)$$
$$C = 1 - \tau_{\mathrm{c}}/S_{\mathrm{u}}; \quad \gamma_{\mathrm{ref}} = S_{\mathrm{u}}/G_{\max}$$
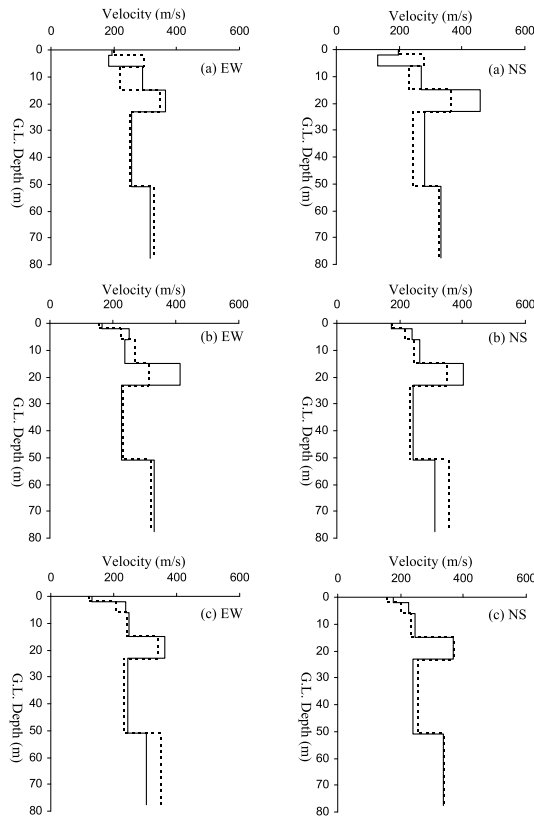
Fig. 10. Shear velocity structures before (continuous traces) and after (dashed traces) the (a) 1993 Kushiro-Oki, (b) 1994 Hokkaido Toho-Oki and (c) 2003 Tokachi-Oki earthquakes.
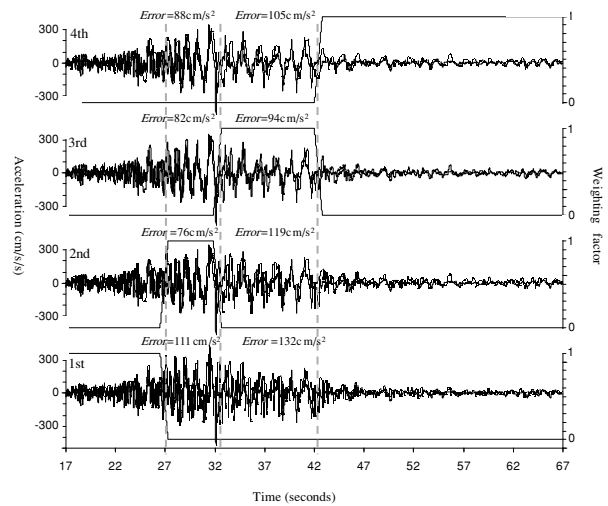

Fig. 11. Nonlinear simulations for the NS component of the 1993 Kushiro-Oki earthquake using moving time-window technique (four time windows), observed (blue traces) and simulated (red traces). Error is the calculated matching error between the observed and the simulated waveforms using the current proposed matching technique (see Eq. (1) through Eq. (4)) at the corresponding time intervals for 1st, 2nd, 3rd, and 4th time windows.
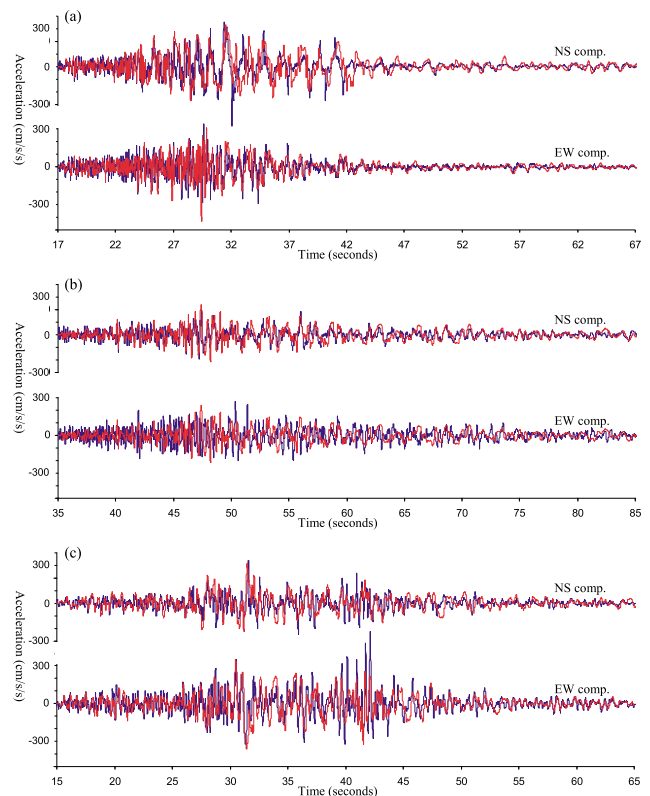

Fig. 12. Nonlinear simulations at Kushiro Port site (0 m depth) for the (a) 1993 Kushiro-Oki, (b) 1994 Hokkaido Toho-Oki, and (c) 2003 Tokachi-Oki earthquakes, observed (blue traces) and simulated (red traces).

where τ is the shear stress, G_{max} is the maximum shear modulus, γ is the shear strain, τ_c and γ_c are the values of the shear stress and shear strain at load reversal, respectively, C and γ_{ref} are parameters controlling the failure-seeking component, and S_u is failure shear strength.

Based on these results, we propose a new technique to account for liquefaction effects and to overcome the misfit along the mainshock time series. Stacking of the simulated weighted waveforms leads to the results shown in Fig. 12, which show excellent agreement with the observations. It is important to note that when the linear or nonlinear simulations are carried out, the resulting simulated waveforms represent the overall response of the entire analyzed lithological column. For example, the predominant periods of the entire lithological column that are shown in Table 2 are 1.2 s, 1.3 s, 1.5 s and 1.7 s for the first, second, third and forth time windows, respectively. Therefore, the shallower layers whose thicknesses are thinner than 10 m can be resolved but included in the entire analyzed lithological column. The analyzed seismic phases in this study are considered to be *S*-waves. A similar assumption was made Aguirre and Irikura (1997) when they analyzed ground motion records of the 1995 Hyogo-ken Nambu earthquake at Port Island vertical array site.

Kokusho and Matsumoto (1998) concluded that damping ratios for the 1995 Hyogo-ken Nambu earthquake are evidently larger than those for the aftershocks. Results obtained by Pease and O'Rourke (1997) from investigations on the seismic response at Treasure Island during the

1989 Loma Prieta earthquake ($M_w = 6.9$) also show that the character of the stress-strain curve drops abruptly after the first 12 s. The present study shows similar results to those obtained by previous researchers in terms of stiffness degradation phenomena that occurs during the liquefaction-
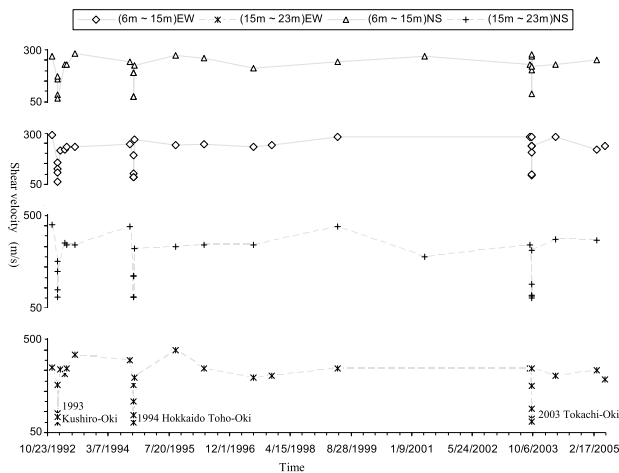
Fig. 13. Schematic representation of the velocity variation at Kushiro Port array site using linear analyses inferred from EW and NS components for the third and fourth layers. Shear velocities estimated during nonlinear analyses have been included for reliable comparison along the velocity variation history.
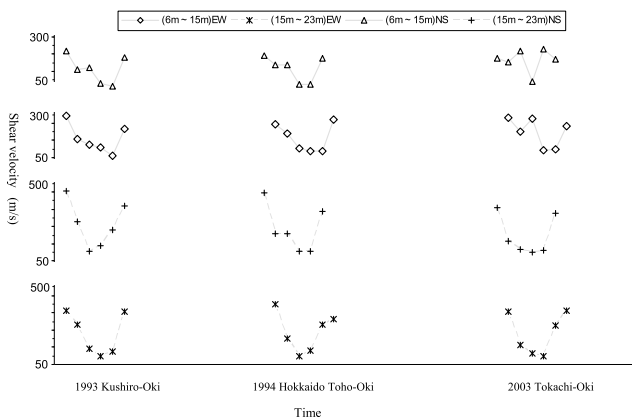

Fig. 14. Schematic representation of the velocity variation at Kushiro Port array site using nonlinear analyses inferred from EW and NS components for the third and fourth layers. It is important to note that the two shear velocity values at the boundary of each curve represent the velocities estimated from two events before and after each mainshock.

induced nonlinear response.

In Figs. 13 and 14, shear velocity variations using linear and nonlinear analyses at Kushiro Port for the layers (6 ∼ 15 m depth and 15 ∼ 23 m depth) show temporarily strong velocity reduction during the three strong ground motions. The velocity variation before, during, and after the three strong motions follows the same tendency as the curve of consolidation shown by Terzaghi (1956).

Although the 2003 Tokachi-Oki earthquake has higher PGA at 77.45 m and shortest epicenter distance compared with the 1994 Hokkaido Toho-Oki earthquake, weak degree of liquefaction appears in the 2003 Tokachi-Oki earthquake, whereas high degree of liquefaction appears in the 1994 Hokkaido Toho-Oki earthquake. As shown in Fig. 10, the shear wave velocity of the fourth layer is highly reduced after the 1993 Kushiro-Oki earthquake and the 1994 Hokkaido Toho-Oki earthquake, whereas after the 2003
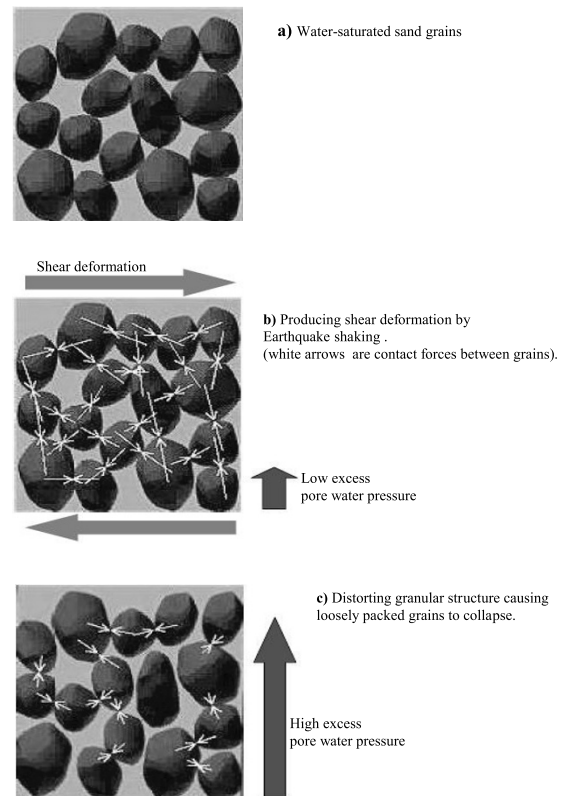

Fig. 15. Schematic representation for liquefaction mechanism in water-saturated sand.

Tokachi-Oki earthquake is slightly reduced. The maximum reductions in shear velocities before and after the 1993 Kushiro-Oki and 1994 Hokkaido Toho-Oki earthquakes are 20% and 24%, respectively, whereas the maximum reduction in shear velocities before and after the 2003 Tokachi-Oki is 6%. This could be attributed to the high increase in rigidity along 9 years (i.e. period between the 1994 Hokkaido Toho-Oki earthquake and the 2003 Tokachi-Oki earthquake).

7. Conclusions

According to previous studies conducted by Kostadinov and Yamazaki (2001) and with the results of our STFT analysis for the observed horizontal ground motions, liquefaction can occur during the mainshocks due to abrupt changes in the predominant frequency. Liquefaction is a process by which sediments below the water table temporarily lose strength gradually and behave as a viscous liquid rather than as a solid, as shown in Fig. 15. We have studied this variation process in stiffness due to the influence of liquefaction by means of a newly proposed nonlinear GA inversion technique applied on records before, during and after the 1993 Kushiro-Oki, 1994 Hokkaido Toho-Oki and the 2003 Tokachi-Oki earthquakes in Hokkaido, Japan. Based on the results of this study, the following conclusions are derived:

1. The proposed inversion technique is more efficient in terms of its estimation ability for shear velocities.
2. Layers (6–23 m depth) exhibited strong reduction in shear velocities during the three successive mainshocks.

3. Stiffness degradation could be evaluated during main-shocks by means of nonlinear GA inversion and then applying moving time-window weighted functions to the nonlinearly simulated waveforms. In this regard, each mainshock is considered to consist of several time-windows. Consequently, each timewindow is considered as an independent motion and has its own nonlinear stiffness parameters.

4. High increase of rigidity following a trend that resembles a consolidation curve could be seen after the 1994 Hokkaido Toho-Oki earthquake. Therefore, a weak degree of liquefaction appears in the 2003 Tokachi-Oki earthquake.

It is hoped that this study will draw increased attention to this topic so as to improve current understanding.

References

Aguirre, J. and K. Irikura, Nonlinearity, Liquefaction, and velocity variation of soft soil layers in Port Isalnd, Kobe, during the Hyogo-ken Nanbu Earthquake, *Bull. Seismol. Soc. Am.*, **87**, 1244–1258, 1997.

Coley, D. A., *An Introduction to Genetic Algorithms for Scientists and Engineers*, World Scietific, 2001.

Coley, D. A., David Coley's GA: http://www.ex.ac.uk/cee/ga/software.htm, 2002.

Koketsu, K., K. Hikima, S. Miyazaki, and S. Ide, Joint Inversion of Strong Motion and Geodetic Data for the Source Process of the 2003 Tokachi-oki, Hokkaido, Earthq., *Earth Planets Space*, **55**, 1–6, 2003.

Kokusho, T. and M. Matsumoto, Nonlinearity in site amplification and soil properties during the 1995 Hyogo-Ken Nanbu Earthquake, *Special Issue of Soils and Foundations*, *Japanese Geotechnical Society*, 1–9, Sept. 1998.

Kostadinov, M. and F. Yamazaki, Detection of soil liquefaction from strong motion records, *Earthq. Eng. Struct. Dyn.*, 173–193, 2001.

Miyajima, M., M. Kitaura, and S. Nozu, Detective method of liquefaction using strong ground motion records, *Proceedings of the 3rd China-Japan-US Trilateral Symposium on Lifeline Earthquake Engineering*, Kunming, China, 133–140, August 1998.

Nakayama, W., Y. Shimizu, and T. Suzuki, A new method to detect subsoil liquefaction using seismic records, *Proceedings of the 53rd Annual Conference of Japanese Society of Civil Engineers*, **vol. 1-B.** JSCE, 862–863, 1998 (in Japanese).

Ozaki, R., Study on real-time earthquake mitigation liquefaction monitoring and earthquake countermeasures, PhD Thesis, Kobe University, 1999 (in Japanese).

Pease, J. W. and T. D. O'Rourke, Seismic response of liquefaction sites, *J. Geotech. Geoenviron. Eng.*, **123**, 37–45, 1997.

Pestana, J. M. and F. Nadim, AMPLE2000 A computer program for analysis of amplification of earthquakes, *Geotechnical Engng. Report No. UCB/GT/2000-04*, Department of Civil & Environ. Engineering, University of California, Berkeley, 2000.

Pyke, R., Non-linear soil models for irregular cyclic loadings, *J. Geotech. Eng. Div.*, ASCE, **105**(GT6), 715–726, 1979.

Qian, Sh. and D. Chen, *Joint Time-Frequency Analysis: Methods and Applications, Prentice-Hall PTR: Upper Saddle River*, NJ, 1996.

Seed, H. B., R. T. Wong, E. M. Idriss, and K. Tokimatsu, *Moduli and Damping Factors for Dymanic Analyses of Cohesionless Soils, Report No. UCB/EERC-84/11*, Erathquake Engineering Research Center, University of California, Berkeley, 1984.

Terzaghi, K., *Theoretical Soil Mechanics*, Wiley, New York, 1956.

Thabet, M., H. Nemoto, and K. Nakagawa, Reliability of shear wave velocity models inferred from linear site response analyses using log data, *J. Geosci.*, *Osaka City Univ.*, **50**, **Art. 9**, p. 107–123, March 2007.

M. Thabet (e-mail: mostafa@sci.osaka-cu.ac.jp), H. Nemoto, and K. Nakagawa